Available online at www.sciencedirect.com

SciVerse ScienceDirect

journal homepage: www.elsevier.com/locate/he

Development of a stable high-aluminum austenitic stainless steel for hydrogen applications

M. Martin [a,*], S. Weber [a,b], W. Theisen [a], T. Michler [c], J. Naumann [d]

[a] Ruhr-Universität Bochum, Institut für Werkstoffe, Lehrstuhl Werkstofftechnik, D-44780 Bochum, Germany
[b] Helmholtz-Zentrum Berlin für Materialien und Energie GmbH, D-14109 Berlin, Germany
[c] Adam Opel AG, Ruesselsheim, Germany
[d] BMW AG, Munich, Germany

ARTICLE INFO

Article history:
Received 5 November 2012
Received in revised form
11 February 2013
Accepted 25 February 2013
Available online 4 April 2013

Keywords:
High-aluminum austenitic stainless steel
Hydrogen environment embrittlement
Austenite stability
Strain-induced martensite
Alloy development

ABSTRACT

A novel high-aluminum austenitic stainless steel has been produced in the laboratory with the aim of developing a lean-alloyed material with a high resistance to hydrogen environment embrittlement. The susceptibility to hydrogen environment embrittlement was evaluated by means of tensile tests at a slow strain rate in pure hydrogen gas at a pressure of 40 MPa and a temperature of −50 °C. Under these conditions, the yield strength, tensile strength and elongation to rupture are not affected by hydrogen in comparison to companion tests carried out in air. Moreover, a very high ductility in hydrogen is evidenced by a reduction of area of 70% in the high-pressure and low-temperature hydrogen environment. The lean degree of alloying is reflected in the molybdenum-free character of the material and a nickel content of 8.0 wt.%. With regard to the alloy concept, a combination of high-carbon, high-manganese, and high-aluminum contents confer an extremely high stability against the formation of strain-induced martensite. This aspect was investigated by means of in-situ magnetic measurements and ex-situ X-ray diffraction. The overall performance of the novel alloy was compared with two reference materials, 304L and 316L austenitic stainless steels, both industrially produced. Its capability of maintaining a fully austenitic structure during tensile testing has been identified as a key aspect to avoid hydrogen environment embrittlement.

Copyright © 2013, Hydrogen Energy Publications, LLC. Published by Elsevier Ltd. All rights reserved.

1. Introduction

The use of hydrogen for power generation in mobile and stationary applications is generally considered to be a very promising alternative among renewable and carbon-free energy sources. Nevertheless, the development of hydrogen energy is limited by the high costs associated with the few materials that guarantee safe handling of hydrogen. In this regard, most metallic materials suffer deterioration of their mechanical properties and ductility on coming into contact with any hydrogen source. This phenomenon is known as hydrogen embrittlement [1]. Therefore, current hydrogen applications make use of high-alloyed austenitic stainless steels, such as AISI type 316 and 310, which show a high resistance to hydrogen embrittlement [2–7]. However, these alloys represent an expensive solution due to their high nickel and molybdenum contents. As a consequence, new steels with equivalent properties but lower associated costs are

* Corresponding author.
E-mail address: martin@wtech.rub.de (M. Martin).
0360-3199/$ – see front matter Copyright © 2013, Hydrogen Energy Publications, LLC. Published by Elsevier Ltd. All rights reserved.
http://dx.doi.org/10.1016/j.ijhydene.2013.02.127

needed. Such materials could support the sustainable development of hydrogen energy on a global scale, which will demand a huge infrastructure for hydrogen production, storage, distribution, and end-use applications.

For decades, the use of austenitic stainless steels in hydrogen applications has gained major attention due to their higher performance compared to other metallic materials [8–10]. More specifically, if the susceptibility to hydrogen environment embrittlement (HEE) is evaluated, both former and present literature agree on the fact that stable austenitic stainless steels show higher resistance to HEE [2,3,5]. In this context, the term "stable" refers to the property of avoiding the formation of α' and ε-martensite under the applied strain at a given temperature. Whereas ε-martensite is assumed to play a minor role in HEE [11,12], the formation of α'-martensite is always accompanied by detrimental effects. In particular, higher ductility losses are encountered for higher tendencies to undergo strain-induced α'-martensite transformation [2–5,13–15]. The latter is frequently associated with the higher diffusivity of hydrogen in the bcc lattice and its enhanced transport through the fast diffusion paths represented by the transformed structure [16,17]. Several investigations have focused on increasing the stability of austenitic stainless steels by modifying the content of interstitial and substitutional elements [6,18–20]. These studies have revealed that increasing the austenite stability has a beneficial impact on the ductility response of the material in a hydrogen environment. This can be interpreted not only on the direction of mitigating the formation of strain-induced α'-martensite, but also on the relationship between austenite stability and the corresponding stacking fault energy (SFE) of the material. Specifically, an increasing SFE will favor more homogenous deformation by means of cross-slip instead of the planar slip mechanism that is promoted by low SFE values [19,21–23].

The need to combine cost reduction with a high resistance to HEE has motivated the identification of a minimum-required nickel content, specially, in modified AISI type 316 steel. The minimum value has been found between 11.5 and 13 wt.%, depending on the testing conditions [19,20,24,25], which is still too high concerning cost-efficiency. Beyond this strategy of minimizing the nickel content in AISI type 316 austenitic stainless steel, not many contributions are encountered in the literature concerning lean-alloyed and HEE-resistant steels. One of the earliest contributions in this context corresponds to the work published by Louthan and Caskey in 1976 [8]. They proposed a 21Cr-6Ni-9Mn stainless steel, commercially known as Nitronic 40, as a possible candidate for hydrogen applications. This material represents a very interesting case of a low-nickel austenitic stainless steel that does not form strain-induced α'-martensite at room temperature [26]. As shown in Ref. [8], the tensile properties of the 21-6-9 steel are equivalent after testing in 69 MPa hydrogen and helium gas at room temperature. However, the same work reports a reduction in ductility response of about 50% after tensile tests of thermally precharged specimens in air at room temperature. A more detailed characterization of this alloy was published by West and Louthan in 1982 [27], in which nineteen different fabrication routes were investigated in the thermally precharged and uncharged condition by means of tensile testing at a strain rate of $5.4 \cdot 10^{-4}\ s^{-1}$ at room temperature. Tensile tests of the uncharged specimens in the annealed condition in 120 MPa hydrogen led to a loss of ductility of around 30% according to values of the reduction of area. The authors concluded "*this austenitic stainless steel is susceptible to hydrogen-induced cracking at grain boundaries, slip bands, and other interfaces*" [27]. A more recent investigation on elastic–plastic fracture mechanics of 21-6-9 performed by Nibur et al. shows a significant reduction in the fracture initiation toughness and crack-growth resistance of thermally precharged specimens [28]. As discussed in detail by the authors, a high concentration of hydrogen can modify the fracture mechanisms in the 21-6-9 stainless steels. Moreover, taking into account the absence of the strain-induced martensitic transformation, the hydrogen-assisted fracture can be interpreted by means of deformation mechanisms that promote localization of deformation [28,29].

Another candidate alloy for use in hydrogen applications is the 22Cr-13Ni-5Mn steel, also introduced by Louthan and Caskey in Ref. [8]. This material exhibits very attractive properties because it combines a high stability against strain-induced martensite formation, a high strength due to nitrogen addition, and a high fracture toughness in the hydrogen precharged condition [30]. The only drawback of this alloy for hydrogen applications could be cost restrictions driven by the relatively high nickel content. Continuing with the idea of combining a stable austenitic matrix, high strength, and high ductility, Cr–Mn–N austenitic steels have also been evaluated with regard to their susceptibility to HEE. In this case, the replacement of nickel by manganese and nitrogen addition proved to be unsuccessful in slow strain rate tensile tests carried out in a 10 MPa hydrogen atmosphere at −50 °C [31]. Specifically, the ductility response of the material was severely reduced, despite the negligible fraction of material that is transformed into strain-induced α'-martensite. The brittle behavior was mainly attributed to the role of nitrogen in promoting short-range ordering and therefore a higher degree of planar slip during deformation [31–34].

The goal of this study was to design a lean-alloyed and HEE-resistant austenitic stainless steel as a potential candidate for high-pressure hydrogen applications at both room temperature and subzero temperatures. The novel alloy was empirically developed and qualified by means of slow strain rate tensile tests in high-pressure hydrogen gas. Being aware of the dependency of HEE-susceptibility on the temperature and strain rate [5,13,25,35–39], the developed material and the reference alloys (304L, 316L) were tested at −50 °C, $5.5 \cdot 10^{-5}\ s^{-1}$ and 40 MPa of pure hydrogen gas, which represents a condition of maximum susceptibility to HEE.

2. Experimental

2.1. Alloying concept

The first decision made concerning the novel material was to take the nominal composition of a lean-alloyed austenitic steel, *e.g.* AISI type 304, as the basis for developing the alloy. This decision relies on the general trend that austenitic stainless steels show a higher resistance to hydrogen embrittlement

than ferritic steels [4,6,8–10]. Three different aspects were considered as milestones for the alloying concept: a) sufficient thermodynamic stability to ensure a fully austenitic phase at industrial solution-annealing temperatures, b) sufficient austenite stability against strain-induced α' formation, and c) a relatively high SFE. The need for a broad austenitic phase field at standard annealing temperatures was required to provide an austenitic microstructure after quenching, which can be also obtained by industrial processing. For the second aspect, avoiding the strain-induced martensitic transformation is considered to be a mandatory step in the alloy development process. Although it is known that a fully stable material does not guarantee a high resistance to HEE [15,31,40], it is also well known that no resistance to HEE is possible in the case of metastable alloys [5,13–15,26]. For the third aspect, featuring a relatively high SFE was understood as a necessary characteristic to be added onto the stability of the alloy. Specifically, a high SFE is expected to lead to a more homogenous deformation by suppressing planar slip [19,22,28,41]. In this context, the possibility of undergoing homogenous deformation is interpreted as a vital issue for counteracting the effect of hydrogen during hydrogen-assisted fracture, which consists of localization of deformation [29,36,42–46].

In this work, and in order to fulfill the aforementioned requirements, five elements of interest were identified as the main components of the alloy, namely: carbon, manganese, chromium, nickel, and aluminum. Subsequently, the pointed composition presented in Table 1 was defined with the support of thermodynamic calculations (CALPHAD method [47–49]). The new alloy is identified as "10-8-2.5" in accordance with the pointed addition of the elements manganese, nickel, and aluminum, respectively.

2.1.1. *Role of the alloying elements*

As can be seen in Table 1, the 10-8-2.5 steel is a high **carbon**-alloyed steel. The intention was to maximize the carbon content because it is beneficial for the three aspects mentioned in Section 2.1. Namely, it increases not only the thermodynamic stability of the austenite at solution-annealing temperatures [50], but also the mechanical stability against α' formation. The last can be deduced from the contribution of carbon in the expression of the M_{d30} temperature in Equation (1). This formula allows to estimate the temperature at which a true strain of 30% is sufficient to transform 50% of the austenite into martensite [51]. Accordingly, the lower the value of the M_{d30} temperature the more stable is the alloy against the strain-induced transformation to α'. Moreover, the addition of carbon is also known to increase the SFE of the material [52,53]. In the case of **chromium** alloying, increasing its content would provide a higher stability against α' formation (Equation (1)), but it would also decrease the SFE and the thermodynamic stability of the fcc phase in the steel [50]. A higher priority was thus given to the detrimental effect of chromium on the SFE of austenitic stainless steels [52,54]. Therefore, its content was reduced to a "minimum allowable" level of 13 wt.%. This amount should combine sufficient corrosion resistance, not evaluated here, with a "minimum" ferrite-stabilizing effect at solution-annealing temperatures. The use of **aluminum** as an alloying element is based on the aim of increasing the SFE of the material. Aluminum is known to have a strong and positive effect on this property [55,56]. Since a higher priority was given to this effect, a large amount of aluminum (2.5 mass%) was considered to be in the solid solution, despite its ferrite-stabilizing nature at solution-annealing temperatures [50]. Alloying with **manganese** has two positive contributions: firstly, it provides thermodynamic stability to the fcc phase at solution-annealing temperatures [50], and secondly, it increases the stability of the alloy against the α' martensitic transformation (Equation (1)). However, the addition of manganese also has negative aspects: it decreases the SFE in austenitic stainless steels [52,54]. Therefore, greater importance was attributed to the effect of manganese on α' formation and on the thermodynamic stability of the fcc phase. Accordingly, 10 wt.% manganese was added to account for the ferrite-stabilization effect of both chromium and aluminum addition. Finally, to account for cost-efficiency, **nickel** content was kept at the level of an AISI type 304 steel, *i.e.* 8 wt.%, and no **molybdenum** was involved in the alloying process. Beyond optimization of the nickel content to improve the cost-efficiency, an addition of 8 wt.% of this element also contributes positively to the three milestones considered in the development of the novel alloy. Namely, providing thermodynamic stability [50], mechanical stability against α' formation (Equation (1)), and increasing the SFE [52,53,57].

$$\begin{aligned} M_{d30} = & 551 - 462\ \text{wt.\%C} - 9.2\ \text{wt.\%Si} - 8.1\ \text{wt.\%Mn} \\ & - 13.7\ \text{wt.\%Cr} - 29\ \text{wt.\%Ni} - 18.5\ \text{wt.\%Mo} \\ & - 29\ \text{wt.\%Cu} - 68\ \text{wt.\%Nb} - 462\ \text{wt.\%N} \\ & - 1.42(\text{grainsize[ASTM]} - 8.0) \end{aligned} \quad (1)$$

Table 1 – Chemical compositions in wt.% of the alloy 10-8-2.5 and reference materials (AISI type 304L and 316L). Measured values obtained by means of optical emission spark spectrometry on tensile specimens.

Alloy	C	Si	Mn	Cr	Ni	Mo	Al	N	Fe
10-8-2.5[P]	0.12	–	10	13	8	–	2.5	–	bal.
10-8-2.5[m]	0.116	0.05	10.27	12.98	7.93	0.03	2.87	0.020	bal.
304L[m]	0.018	0.70	1.96	17.7	8.6	0.30	0.001	0.075	bal.
316L[m]	0.012	0.83	1.43	17.1	12.5	2.46	0.002	0.057	bal.

[P] Pointed.
[m] Measured.

2.2. *Alloy production and testing*

2.2.1. *Production*

The alloy 10-8-2.5 was produced in the laboratory via ingot casting in a vacuum induction furnace. As-cast ingots with a weight of 3 kg and a diameter of 50 mm were pre-machined down to 42 mm and hot-worked in several passes to a final diameter of 16 mm, followed by water quenching. Six tensile specimens with a gauge length of 30 mm and a diameter of 5 mm were machined out of the center of the as-forged bars by means of wet-turning as described in Ref. [58]. Subsequently, the as-turned specimens were heat-treated in an industrial vacuum furnace for 30 min at 1050 °C, followed by quenching in argon gas at a pressure of 200 kPa. The last step is essential to avoid undesirable contributions of turning operations on

the performance of the material during testing in hydrogen [58]. After the heat treatment, two tensile specimens of alloy 10-8-2.5 were manually polished down to 1 μm by mounting them on a small turning machine to minimize geometric deformations. A total of four specimens were supplied for hydrogen testing (2 polished and 2 without polishing) while the remaining two were employed as references in air atmosphere.

Reference materials were semi-finished bars of austenitic stainless steels AISI type 304L and 316L that were provided by Deutsche Edelstahlwerke (DEW, Germany). Tensile specimens were machined out of the center of a 30 mm diameter bar material and heat-treated in the same batch with the specimens of the alloy 10-8-2.5. Measurements of chemical composition performed on tensile specimens are presented in Table 1 for both reference materials. The aforementioned production route resulted in an average grain size of 45μm ± 5 μm (ASTM grain size number $G = 6.0$) in the three investigated alloys.

2.2.2. Testing

Tensile tests in air and in pure hydrogen gas (≥99.9999% H_2) were carried out with the three materials at −50 °C. Ambient pressure was used for the air-tested specimens, whereas 40 MPa was applied for the tests in a hydrogen atmosphere. For hydrogen testing, the vessel was purged three times with pure nitrogen at 1 MPa. This was followed by eight consecutive purges with pure hydrogen at 1 MPa, and then the vessel was filled to the test pressure. This procedure ensures safety and gas purity. In both air and hydrogen tests, an initial strain rate of $5.5 \cdot 10^{-5}$ s^{-1} was used according to ASTM G129 standard [39]. In the case of the hydrogen tests, the load was measured using an internal load cell in all cases. Clip gauge/extensometer measurements were used in air/hydrogen environments to determine the 0.2% proof stress. Measured properties were yield strength ($R_{p0.2}$), ultimate tensile strength (R_m), and elongation to rupture (A). Additionally, values of reduction of area (Z) were obtained by measuring the initial and final diameters of the specimen at the necking circumference with a digital caliper. The Z parameter is known to be a very sensitive measure of the susceptibility of metallic materials to HEE [5,15,21].

2.3. Characterization

2.3.1. Microstructure and fracture surfaces

Longitudinal sections of the threaded parts in tensile specimens were metallographically prepared by grinding and polishing down to 1 μm with diamond paste. A V2A solution (100 ml H_2O, 100 ml HCl, 10 ml HNO_3) was then employed to reveal the microstructure of the samples. Whereas etched samples were investigated by optical microscopy, samples in the as-polished condition were used for the identification of nonmetallic inclusions by means of energy-dispersive X-ray spectroscopy (EDS) in a LEO 1530-VP scanning electron microscope (SEM).

An initial characterization of the fracture surfaces and necking regions at the macroscopic scale was performed with a VHX-600D digital microscope (Keyence GmbH, Germany). Digital images were obtained in the as-tested condition employing a RZ-20 lens and a light filter with a magnification of 50×. After obtaining a macroscopic image of the rupture, the fracture surfaces were investigated via secondary electron contrast with the SEM.

2.3.2. Austenite stability

Martensite formation during tensile testing was followed in-situ by means of the magnetic induction method using a FeritScope® MP30 device (Helmut Fischer GmbH, Germany). Since preliminary studies had shown that a loaded state influenced the material's magnetic response, measurements were carried out at loads lower than 100 N at increments of 5% engineering strain by interrupting the loading process with an unload/load cycle. This type of measurement was carried out in an air atmosphere at −50 °C. The readings of the instrument, expressed as a ferrite equivalent, were converted into a mass fraction of α'-martensite using a correction factor of 1.7 [59].

A second measurement of strain-induced martensite formation in the bulk material was carried out by means of X-ray diffraction (XRD) on the remaining pieces of the air- and hydrogen-tested specimens. Longitudinal sections were metallographically prepared out of the former gauge lengths. Diffraction patterns were then acquired from a middle point between the fracture surface and the beginning of the gauge length using an XPERT-MPD diffractometer with Cr-K_α radiation in the range of (62°–165°)2θ. The obtained patterns were compared with data for α'- and ε-martensite in type 304 steel published by Narita et al. [60].

3. Results

3.1. Thermodynamic stability

The measured chemical composition of alloy 10-8-2.5, presented in Table 1, was used to calculate the corresponding phase diagram with the Calphad software ThermoCalc S [61] in conjunction with the thermodynamic database TCFe6.2 [62]. The resulting diagram is shown in Fig. 1, in which the dashed line depicts the corresponding carbon isopleth. As can be seen, alloy 10-8-2.5 presents a primary ferritic solidification followed by a two-phase field (bcc + fcc) that becomes a fully austenitic field at 1230 °C. Moreover, the wide austenitic field in both carbon content and temperature ranges indicates sufficient thermodynamic stability. Thus a fully austenitic microstructure can be obtained by means of a solution-annealing treatment followed by rapid cooling. In particular, the material can be treated in the temperature range between 1050 and 1150 °C, which covers standard industrial practices. Likewise, the thermodynamic calculations indicate that stable aluminum nitrides (AlN) are already forming in the melt. Since the occurrence of this phase is due to residual nitrogen content (always present in laboratory-scale production), a small and not relevant volume fraction of AlN can be expected in the microstructure of the material.

3.2. Microstructure and mechanical testing

Prior to testing, all specimens showed a typical austenitic microstructure as a result of the production process described

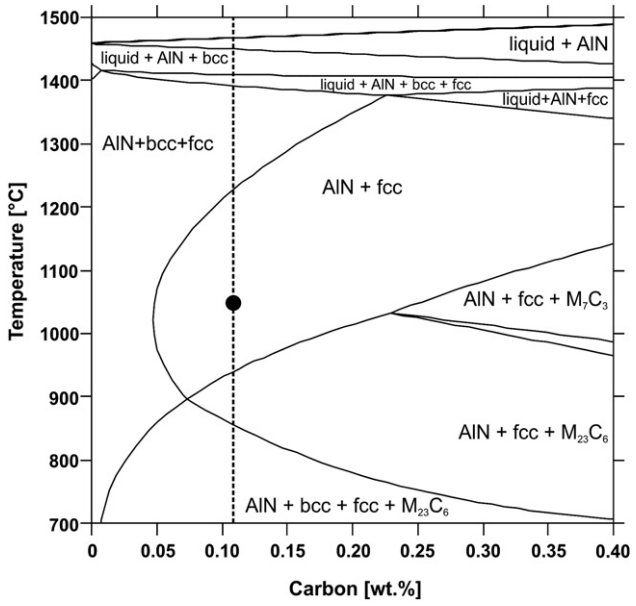

Fig. 1 – Calculated phase diagram of the alloy 10-8-2.5. The spot indicates the temperature employed during solution annealing.

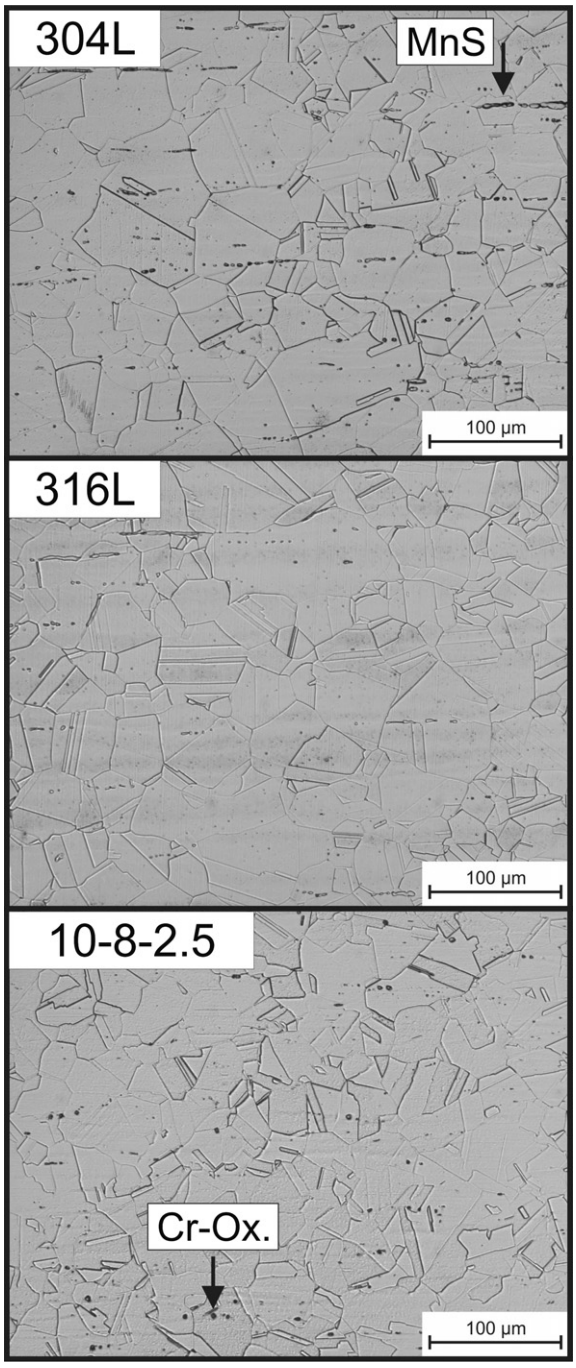

Fig. 2 – Optical micrographs of reference materials and steel 10-8-2.5. The presence of chromium oxides was identified in the novel alloy by means of EDS analysis.

in Section 2.2. Common features among the three alloys were the presence of annealing twins and a grain size of 45μm ± 5 μm. With respect to the reference materials, the 316L showed a cleaner microstructure, whereas the 304L alloy was characterized by a much higher density of manganese sulfides aligned in the rolling direction. Regarding the laboratory heat, although alloy 10-8-2.5 was free of manganese sulfides, it presented a relatively high density of chromium oxides distributed inside the grains. Optical micrographs representative of the three alloys are presented in Fig. 2.

The three alloys were tensile tested at −50 °C in air at atmospheric pressure and in a 40 MPa hydrogen gas atmosphere, as described in Section 2.2.2. Exemplary tensile curves are shown in Fig. 3 for both atmospheres, in which a first difference among the investigated materials can be deduced from the appearance of the tensile curves. A marked strain-hardening is observed for the AISI type 304L steel, whereas the 316L and 10-8-2.5 alloy show a steady and more ductile stress/strain response. A comparison of the tensile curves in both atmospheres reveals that tensile strength and elongation to rupture are severely reduced by hydrogen in the case of the 304L steel, whereas the alloys 316L and 10-8-2.5 show equivalent performances in air and hydrogen. Moreover, very similar curves were registered in a hydrogen atmosphere for the 10-8-2.5 alloy and the reference AISI type 316L steel.

The values of the tensile properties associated with the previous curves are presented in Table 2, together with the calculation of reduction of area (Z), as the average value of two tests performed under the same conditions. The extra set of average values for the manually polished specimens of alloy 10-8-2.5 is also included. The results in Table 2 indicate that the yield strength is not affected in any case by tensile testing in external hydrogen. Additionally, the detrimental effect of hydrogen in the case of AISI 304L becomes more evident on the basis of the measured values of R_m, A and the calculated Z. On the other hand, alloys 316L and 10-8-2.5 show no detrimental effect on the tensile strength and elongation to rupture caused by the presence of hydrogen. The only parameter that is slightly lower in both cases is the reduction of area (Z). In this regard, the variant of the polished specimens of alloy 10-8-2.5 tested in gaseous hydrogen shows an improved response with respect to the reduction of area with a lower elongation to rupture.

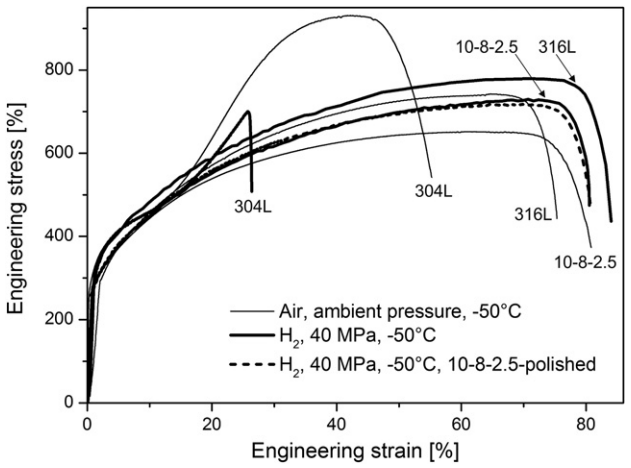

Fig. 3 – Engineering stress/strain curves of alloys 304L, 316L, and 10-8-2.5 obtained at −50 °C in air (atmospheric pressure) and 40 MPa hydrogen gas.

In addition to the values of the reduction of area, a direct impression of the ductility response of the three alloys is obtained from the macroscopic image of the necking regions of the as-tested specimens shown in Fig. 4. This observation exemplifies the macroscopic brittle behavior of the AISI type 304L steel, and the very high ductility of the reference material 316L and the novel alloy 10-8-2.5. At this magnification, it is possible to identify the presence of transverse cracks on the fracture surface of alloy 10-8-2.5 that are not visible on the 316L steel. On the other hand, the polished specimens of alloy 10-8-2.5 showed a typical cup-and-cone rupture in hydrogen atmosphere with a fracture surface free of transverse cracks, as depicted in Fig. 5.

3.2.1. *Austenite stability*

Primary characterization of the austenite stability of the three investigated alloys was carried out by means of bulk measurements aimed at detecting the presence of ferromagnetic phases. A FeritScope® MP30 device was employed for measuring ferrite equivalent values during tensile testing in air at −50 °C, which were later transformed into mass percentages of α'-martensite (see Section 2.3.2). The resulting curves are shown in Fig. 6. As can be seen, all materials start with a value of zero mass percent for zero strain, which means a fully austenitic structure at the start of the tensile test. As the test progresses, two tendencies are immediately identified: firstly, the low stability of the AISI type 304L for engineering strains higher than 10%, and secondly, the very stable evolution of alloys 316L and 10-8-2.5 with deformation. Concerning the last two materials, the corresponding α' percentages remain close to zero up to an engineering strain of 45%. Starting from 50% strain onwards, the 316L alloy deviates toward higher values to end up with 6.1 mass% of α' for the last reading. Alloy 10-8-2.5 shows a more stable structure than the 316L steel, with 1.8 mass % of α'-martensite for the last ferrite equivalent reading.

In addition to the magnetic response measurements, X-ray diffraction analyses were carried out on longitudinal sections of the air- and hydrogen-tested specimens to account for the formation of α'- and ε-martensite. The results presented in Fig. 7 allow the identification of the phases γ and α, without any significant contribution of the ε phase.

According to the intensity of the α-reflections, alloy 304L appears to be much less stable, whereas the presence of α'-martensite can be identified in the 316L steel at the consecutive α-reflections. Fig. 7 also shows the alloy 10-8-2.5 to be the most stable of the three materials. It features an almost fully austenitic structure. In addition, the X-ray diffraction analyses show that the testing environment has no impact on the formation of α'-martensite in the alloys 316L and 10-8-2.5. On the contrary, the formation of α' is more pronounced in the air atmosphere with respect to hydrogen for the 304L alloy. This can be correlated to the higher deformation degree that is introduced in air atmosphere. Specifically, a uniform elongation of A = 53% in air and A = 25% in hydrogen (Table 2). Similarly, a very good correlation is found between X-ray diffraction patterns and the magnetic induction method with respect to α' formation in the bulk material.

Table 2 – Mechanical properties of the reference materials 304L/316L and the novel alloy 10-8-2.5. Tensile tests performed at −50 °C in air at atmospheric pressure and in 40 MPa hydrogen gas with an initial strain rate of $5.5 \cdot 10^{-5}$ s^{-1}. Average values of two tests performed in the same condition.

Alloy	$R_{p0.2}$ [MPa]		R_m [MPa]		A [%]		Z [%]	
	H_2	Air	H_2	Air	H_2	Air	H_2	Air
304L	300	284	720	929	25	53	17	77
316L	316	298	783	727	81	73	75	80
10-8-2.5	276	256	711	656	79	78	70	83
10-8-2.5[a]	283	n.d.	713	n.d.	73	n.d.	75	n.d.

n.d., not determined.
a Polished surface.

3.3. *Fractography of alloys 10-8-2.5 and 316L*

Fractographic analyses were carried out on the three alloys to compare rupture in a hydrogen atmosphere with the corresponding failure in air. All the air-tested specimens exhibited a dimpled rupture of the cup-and-cone type. Since Fig. 4 clearly exemplifies the type of rupture of the three alloys in air, only the fractography of alloy 10-8-2.5 is presented for this testing condition in Fig. 8. This figure shows secondary electron images of three regions of interest that are numbered according to the low magnification image on the top left. These regions cover the center of the necked region (1), an intermediate radial zone (2), and the outer shear-lip (3). This selection corresponds to the three stages of tensile fracture that occur consecutively and which are: initiation and growth of a central crack in 1, propagation along shear planes in 2, and termination of the fracture in region 3 [63–65]. As can be seen in Fig. 8, the material fails due to microvoid coalescence in region 1 with deep and equiaxed dimples. In region 2, ductile propagation is also evidenced by shallow and equiaxed dimples. Termination of the fracture also occurs in a ductile manner with the presence of elongated dimples having an open end as a special feature. The fact that the open end of the dimples faces the surface of the specimen indicates that

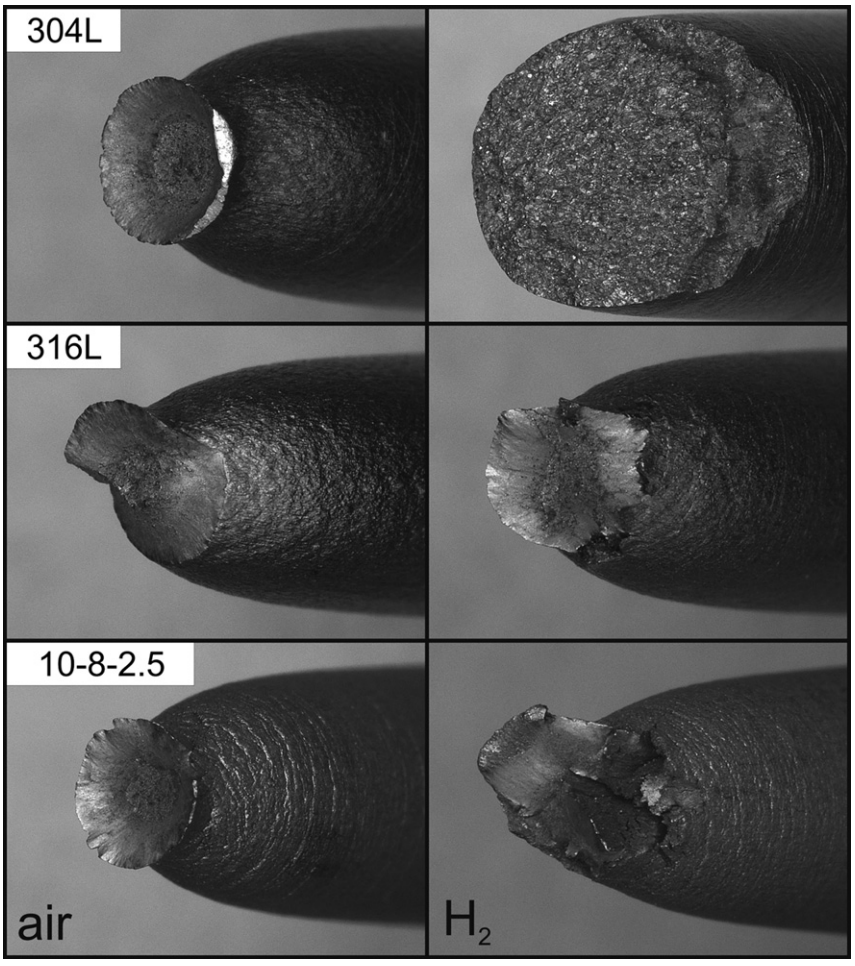

Fig. 4 – Macroscopic image of the necking area and fracture surface of reference materials and alloy 10-8-2.5 after testing at −50 °C. Air at atmospheric pressure (left), 40 MPa hydrogen gas (right).

fracture propagation occurs from the center toward the outer region, as indicated by the arrow in Fig. 8-3 [65].

In contrast to the air case, the hydrogen-tested specimens of alloy 10-8-2.5 feature mixed failure with outer zones showing hydrogen-assisted-like fracture and dimpled rupture in the rest of the fracture surface, as shown in Fig. 9. Areas with indications of hydrogen-assisted fracture are identified with the number 3 and are highlighted by hatched lines in the low magnification picture. The hydrogen-affected areas are distributed around the border of the fracture surface and are separated from each other. They represent about 23% of the

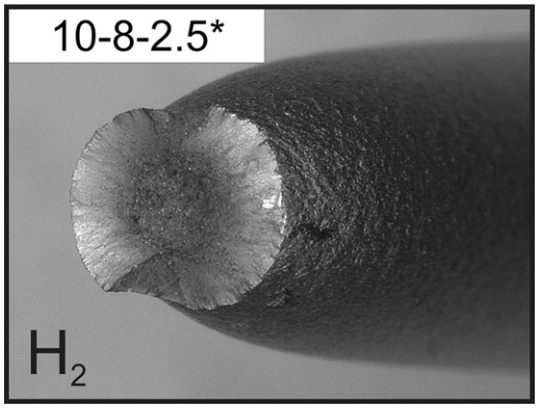

Fig. 5 – (*) Polished specimen of alloy 10-8-2.5 after testing at −50 °C in 40 MPa hydrogen gas.

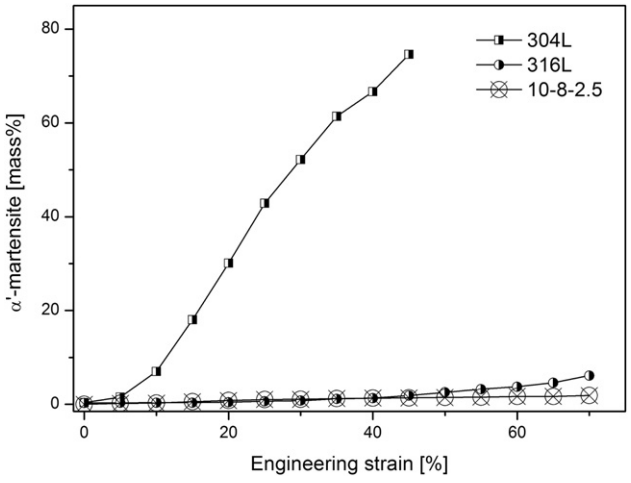

Fig. 6 – *In-situ* measurement of strain-induced α′-martensite formation during tensile testing in air at −50 °C, atmospheric pressure, and an initial strain rate of $5.5 \cdot 10^{-5}$ s^{-1}.

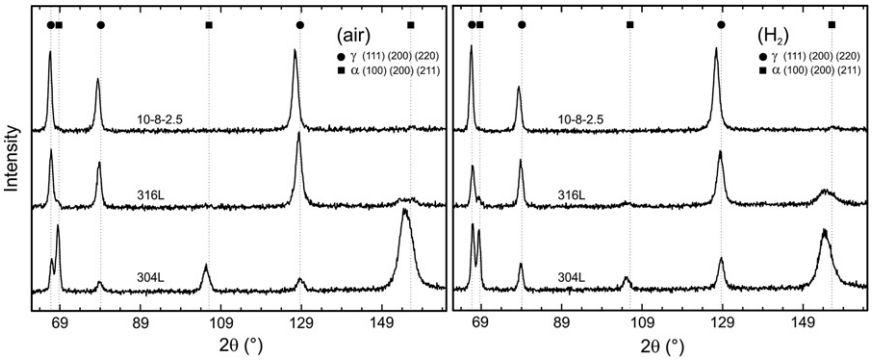

Fig. 7 – X-ray diffraction patterns of longitudinal sections of alloys 304L, 316L, and 10-8-2.5 after testing in air (left) and 40 MPa hydrogen gas (right) at −50 °C.

whole surface. The rest of the surface shows dimpled rupture but with two different morphologies. Whereas region 2 features a smooth surface with relatively small and shallow dimples, region 1 has an uneven surface and the dimples have a more equiaxed and deeper structure.

Fractographic analysis of the reference materials in hydrogen revealed that 304L has a transgranular cleavage-like failure with some intergranular ruptures (not shown here), whereas the rupture of the 316L steel presents similarities to alloy 10-8-2.5. Specifically, a mixed failure mode is observed with hydrogen-affected regions in the outer regions and dimpled rupture in the rest of the fracture surface. The latter is presented in Fig. 10, in which micrograph 3 shows an example of the hydrogen-assisted-like fracture, and regions 1 and 2 show dimpled rupture. Quantification of the hydrogen-affected area corresponds to about 17% of the surface.

Quite impressive fractographic results were obtained for the polished specimen of alloy 10-8-2.5 presented in Fig. 11. The mixed failure mode observed in Fig. 9 has changed to completely dimpled rupture in the three regions of interest. The failure of the polished specimen in hydrogen is very similar to that in air (Fig. 8), with no indications of hydrogen-assisted fracture at all. Moreover, the fracture surface of the outer shear lip (3) is characterized by elongated open-end dimples that indicate a direction of propagation from the center toward the outer part of the specimen. This coincides with the observations on the air-tested specimens.

4. Discussion

Many years of investigation on HEE of austenitic stainless steels have revealed a correlation between the tendency of the material to undergo strain-induced α'-martensitic transformation and the ductility response in a hydrogen atmosphere. Namely, the ductility of the material in hydrogen

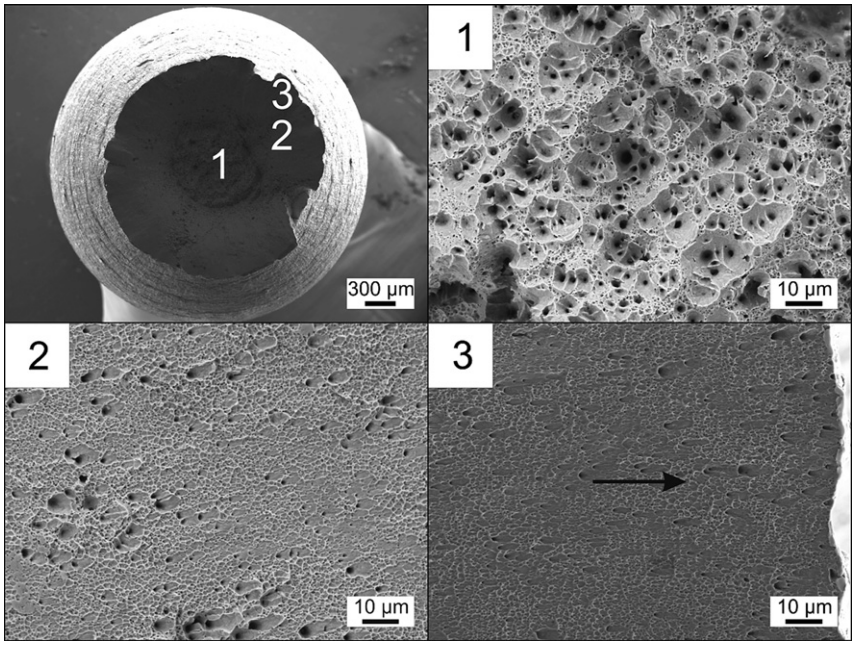

Fig. 8 – Fracture surface of alloy 10-8-2.5 tested at −50 °C in air with an initial strain rate of $5.5 \cdot 10^{-5}$ s^{-1}. The arrow in micrograph 3 indicates the direction of fracture propagation.

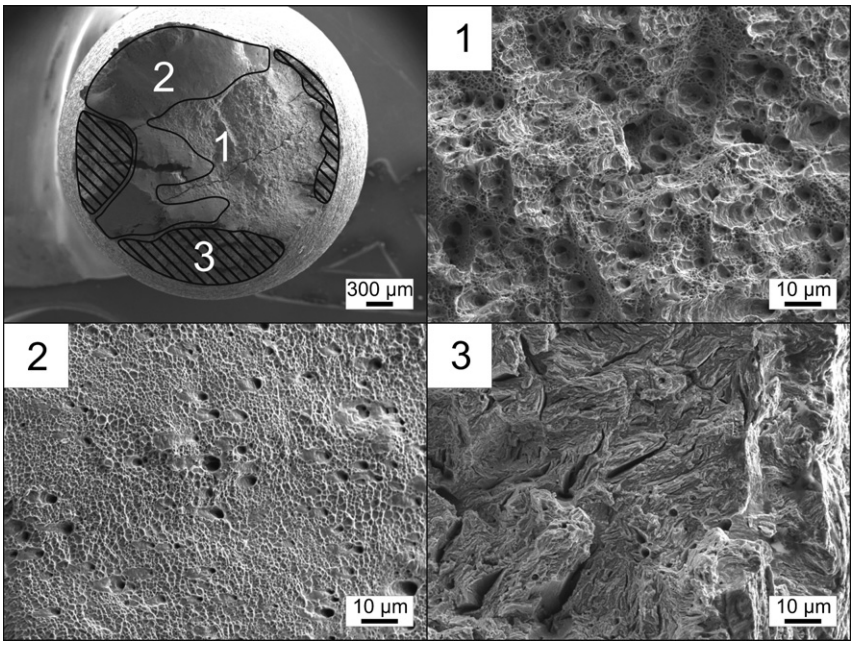

Fig. 9 – Fracture surface of alloy 10-8-2.5 tested at −50 °C in 40 MPa hydrogen gas atmosphere with an initial strain rate of $5.5 \cdot 10^{-5}$ s^{-1}.

decreases with increasing volume fraction of strain-induced α' martensite. Specifically, stable austenitic stainless steels show a high resistance to HEE, whereas metastable steels present a poorer resistance to HEE [2–7,26]. This correlation has led the discussion of HEE in austenitic stainless steels, almost exclusively, to the role of the strain-induced α' transformation. In turn, the strain-induced α' transformation is generally regarded to be a function of the nominal chemical composition of the material, particularly, the nickel content or the corresponding nickel equivalent value. However, the problem of HEE in austenitic stainless steels cannot be reduced to the scope of a nominal composition or a nickel equivalent value. Moreover, for one and the same material the susceptibility to HEE depends on the amount and geometry of segregations [24,66], on heat treatments performed prior to testing [67], and on the effect of turning operations on the

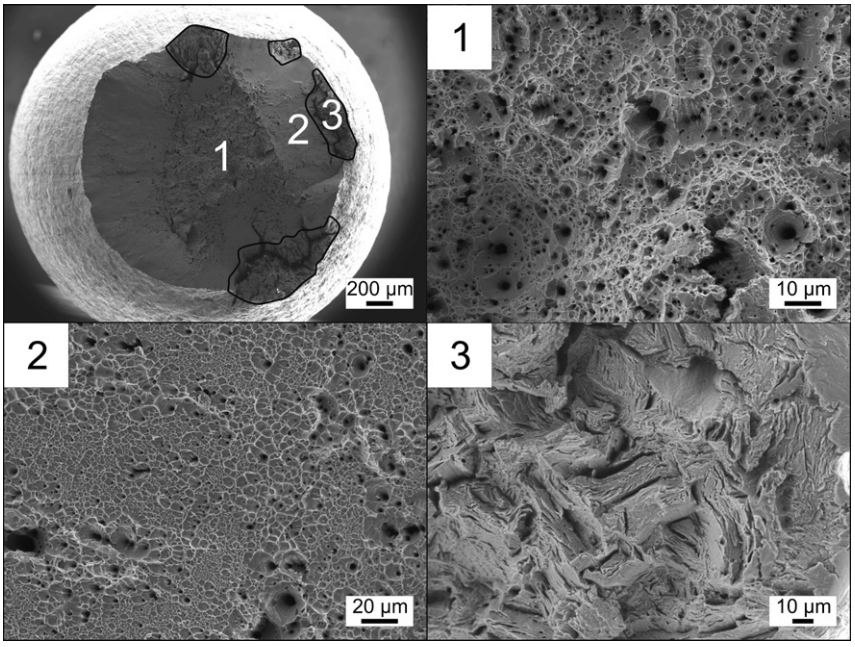

Fig. 10 – Fracture surface of alloy 316L tested at −50 °C in 40 MPa hydrogen gas atmosphere with an initial strain rate of $5.5 \cdot 10^{-5}$ s^{-1}.

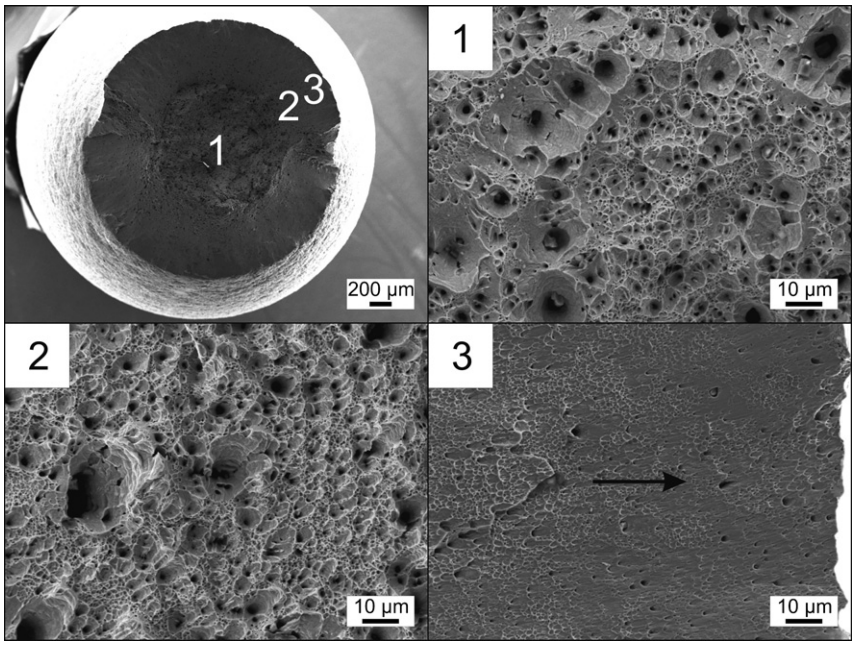

Fig. 11 – Fractographs of a polished specimen of alloy 10-8-2.5 tested at −50 °C in 40 MPa hydrogen gas atmosphere with an initial strain rate of $5.5 \cdot 10^{-5}$ s^{-1}. The arrow in micrograph 3 indicates the direction of fracture propagation.

surface of the material [58]. All these aspects have to be considered together with the occurrence of strain-induced α'-martensitic transformation during the development of HEE-resistant austenitic steels. In this work, the alloy development process was based on three main attributes with allowance for the aforementioned aspects. Specifically, an austenitic microstructure was obtained with a combination of very high stability against the formation of strain-induced α' martensite and the possibility of undergoing uniform deformation by means of a relatively high SFE. Whereas the first two requirements have been verified for the novel alloy 10-8-2.5, the experimental evaluation of both SFE and the corresponding deformation mechanism are part of future investigations. For the alloys investigated in this work, the reference materials 304L and 316L define boundary conditions in terms of poor and high resistance to HEE. The novel alloy can be placed between both limits, but toward the high resistance side *i.e.*, it performs in an equivalent way to the AISI type 316L stainless steel.

The main and most important difference among the alloys investigated in this work relies on the stability of the austenitic phase against strain-induced α'-martensitic transformation. The low stability of the 304L steel was evidenced during the testing and characterization process. The first indication of microstructural changes appears on the tensile curves depicted in Fig. 3,in which strong strain-hardening is observed in both atmospheres. The latter can be directly related to continued transformation of the primary austenitic phase into α'-martensite with increasing deformation, as shown in Fig. 6, and also confirmed by X-ray diffraction (Fig. 7). The occurrence of strain-hardening in the 304L alloy is accompanied by premature failure in hydrogen, characterized by a reduction of 22% in yield strength, 53% in elongation to rupture and 78% in reduction of area, see Table 2. These values together with the overview presented in Fig. 4 clearly prove the high susceptibility of this alloy to HEE. The poor macroscopic ductility observed in the 304L steel has been related to the effect of α' martensite on facilitating the penetration and transport of hydrogen through the material [5,13,14,16,17].

In contrast to the 304L steel, both alloys 316L and 10-8-2.5 show a very high stability against α'-martensite formation, and there was no detrimental effect of external hydrogen on either the tensile strength or the elongation to rupture. Only the reduction of area (Z) was slightly affected in both alloys by the hydrogen gas environment (Table 2). The novel alloy exhibited an increase of 5% in the Z value in a hydrogen atmosphere for the polished variant compared to the as-machined condition, indicating a positive effect due to surface conditioning. More significant than this difference in the Z value is the change in the failure mode occurring between the as-machined and the polished specimens of alloy 10-8-2.5 shown in Figs. 9 and 11. This change can be related to a surface effect associated with the micronotches resulting from the machining process. These micronotches can act as stress concentrators during tensile loading and facilitate hydrogen penetration by modifying the local state of stresses, promoting the formation of plastic zones and the nucleation of dislocations at the surface of the specimen [21]. These conditions are favorable for hydrogen-assisted fracture to occur in the form of superficial cracking [46]. As long as the growth of these superficial cracks is assisted by the external hydrogen, a fracture surface of the type showed in Fig. 9-3 can be expected. Since the novel alloy experiences a very high reduction of area (Table 2) it is quite likely that the hydrogen-assisted fracture at the surface occurs close to the necking of the specimen in terms of time. Thus competition between hydrogen-assisted fracture initiated at the surface and the natural failure of the bulk material is expected to occur. From the fractographs

presented in Fig. 9, it is assumed that development of the hydrogen-assisted zone (3) is arrested at a certain point by the bulk properties of the material, resulting in the change of fracture mode.

A similar reasoning can be applied to the fractographic results of alloy 316L presented in Fig. 10. Namely, an outer part, which is affected by the hydrogen atmosphere at certain positions where the stress concentration is high enough to allow hydrogen penetration, and the bulk material, which is able to arrest progression of the hydrogen-assisted fracture. The higher cleanliness of the alloy 316L (Fig. 2) is expected to play a beneficial role in reducing the stress concentration at the surface of the material. The latter could explain the differences in the hydrogen-affected area between this material and the novel alloy quantified in 17 and 23%, respectively.

Although the beneficial effect of a polished surface on the susceptibility to HEE has been reported in the literature [21,67], the fractographic results presented in Fig. 11 cannot be explained solely on the basis of simple surface conditioning. A completely dimpled fracture is observed for a polished specimen of alloy 10-8-2.5 tested at −50 °C in 40 MPa hydrogen atmosphere. Moreover, the shape, size, and distribution of the dimples are much more similar to those observed on the air-tested specimen compared to those obtained with the as-machined specimens in a hydrogen atmosphere (Figs. 8 and 9). The initiation and propagation of superficial cracks occurring during tensile testing in external hydrogen [46] is expected to be suppressed due to the removal of micronotches during surface conditioning. Therefore, if the generation of superficial cracks is avoided, the material is able to deform in its natural manner *i.e.*, from the center toward the outer part of the specimen [63–65]. This argument is based on observation of elongated open-end dimples in the shear-lip zone in Fig. 11-3, where the direction of the fracture propagation can be identified in the same way as for the specimens tested in air (Fig. 8-3). Taking into account that significant hydrogen uptake cannot occur by means of diffusion for this type of material [16,21,58], the main interaction between the material under deformation and the external hydrogen atmosphere is the ingress of hydrogen atoms that enter dislocations generated on the surface of the material [21]. In this scenario, if the novel alloy is prone to deform by means of cross-slip, the ingressing hydrogen atoms will be distributed in different slip systems and the risk of undergoing localization of deformation will be reduced. Accordingly, if localization of deformation is avoided on the microscopic scale, a ductile macroscopic response can be expected.

The overall performance of the alloy 10-8-2.5 can be primarily understood on the basis of its stability against strain-induced martensitic transformation. Specifically, Figs. 6 and 7 clearly indicate a higher stability of this alloy compared to the reference steel 316L. Nevertheless, other attributes are needed in addition to sufficient austenite stability to obtain a HEE-resistant material [40]. In the case of alloy 10-8-2.5, the possibility of undergoing homogenous deformation under plastic strain was thought to be the necessary extra attribute.

Undoubtedly, further investigations on hydrogen-assisted fracture of alloy 10-8-2.5 are required. In particular, the experimental determination of SFE, a complete description of the deformation mechanism, and the fracture mechanics properties are of major interest to interpret the behavior of this alloy in hydrogen. Nevertheless, the performance of this material in 40 MPa pure hydrogen gas at −50 °C means it is a promising candidate for hydrogen applications.

5. Summary

A novel lean-alloyed austenitic steel with a high resistance to hydrogen environment embrittlement (HEE) was developed in the laboratory by means of an empirical approach. In particular, the combination of high-carbon, high-manganese, and high-aluminum contents is the basis of a molybdenum-free and 8.0 wt. % nickel-containing material. The susceptibility of the alloy to HEE was evaluated by means of slow strain rate tensile testing in a 40 MPa pure hydrogen gas atmosphere at −50 °C, and compared with two commercial AISI type 304L and 316L steels. Under these conditions, the novel alloy showed a high resistance to HEE, which was equivalent to that of the 316L reference material. Primarily, the overall performance of the novel alloy can be understood on the basis of its extremely high stability against strain-induced martensite formation. Moreover, the high ductility of the material in a hydrogen atmosphere suggests a certain capability of undergoing homogeneous deformation under plastic strain. The performance of the novel alloy in hydrogen gas atmosphere means it is a promising candidate for hydrogen applications. Finally, by considering the absence of molybdenum and the reduction in nickel content by more than 4 wt. % compared to the steel 316L, the alloy surcharge is expected to be significantly lower, thus suggesting a cost benefit for components operating in hydrogen environments.

Acknowledgment

The authors gratefully acknowledge the financial support of the Bundesministerium für Wirtschaft und Technologie (BMWi) under contract number 0327802D. Tensile tests in hydrogen were performed at “The Welding Institute” (TWI, Cambridge, UK).

REFERENCES

[1] Birnbaum HK. Hydrogen embrittlement. Encyclopedia of Materials: Science and Technology 2001:3887–9.
[2] Eliezer D, Chakrapani DG, Altstetter CJ, Pugh EN. Influence of austenite stability on the hydrogen embrittlement and stress-corrosion cracking of stainless-steel. Metallurgical Transactions A – Physical Metallurgy and Materials Science 1979;10(7):935–41.
[3] Singh S, Altstetter C. Effects of hydrogen concentration on slow crack-growth in stainless-steels. Metallurgical Transactions A 1982;13(10):1799–808.
[4] Perng TP, Altstetter CJ. Comparison of hydrogen gas embrittlement of austenitic and ferritic stainless-steels. Metallurgical and Materials Transactions A – Physical Metallurgy and Materials Science 1987;18(1):123–34.

[5] Han G, He J, Fukuyama S. Effect of strain-induced martensite on hydrogen environment embrittlement of sensitized austenitic stainless steels at low temperatures. Acta Materialia 1998;46(13):4559–70.
[6] Deimel P, Sattler E. Austenitic steels of different composition in liquid and gaseous hydrogen. Corrosion Science 2008;50:1598–607.
[7] Zhang L, Wen M, Imade M, Fukuyama S, Yokogawa K. Effect of nickel equivalent on hydrogen environment embrittlement of austenitic stainless steels at low temperatures. Fracture of Nano and Engineering Materials and Structures, Proceedings of the 16th European Conference of Fracture.
[8] Louthan MR, Caskey GR. Hydrogen transport and embrittlement in structural metals. International Journal of Hydrogen Energy 1976;1(3):291–305.
[9] Thompson AW. Structural materials use in a hydrogen energy economy. International Journal of Hydrogen Energy 1977;2:299–307.
[10] Ohta T, Abe I. Hydrogen energy research and development in Japan. International Journal of Hydrogen Energy 1985;10(5):275–9.
[11] Shivanyuk VN, Foct J, Gavriljuk VG. On a role of hydrogen-induced epsilon-martensite in embrittlement of stable austenitic steel. Scripta Materialia 2003;49(6):601–6.
[12] Teus SM, Shyvanyuk VN, Gavriljuk VG. Hydrogen-induced gamma- epsilon transformation and the role of epsilon-martensite in hydrogen embrittlement of austenitic steels. Materials Science and Engineering: A 2008;497(1–2):290–4.
[13] Caskey GR. Hydrogen effects in stainless steel. In: Oriani RA, editor. Hydrogen degradation of ferrous alloys 1985. p. 822–62. Noyes, Park Ridge and N.J.
[14] Mine Y, Narazaki C, Murakami K, Matsuoka S, Murakami Y. Hydrogen transport in solution-treated and pre-strained austenitic stainless steels and its role in hydrogen-enhanced fatigue growth. International Journal of Hydrogen Energy 2009;34:1097–107.
[15] Martin M, Weber S, Theisen W, Michler T, Naumann J. Effect of alloying elements on hydrogen environment embrittlement of AISI type 304 austenitic stainless steel. International Journal of Hydrogen Energy 2011;36(24):15888–98.
[16] Perng TP, Altstetter CJ. Effects of deformation on hydrogen permeation in austenitic stainless-steels. Acta Metallurgica 1986;34(9):1771–81.
[17] Kanezaki T, Narazaki C, Mine Y, Matsuoka S, Murakami Y. Effects of hydrogen on fatigue crack growth behavior of austenitic stainless steels. International Journal of Hydrogen Energy 2008;33(10):2604–19.
[18] Michler T, Berreth K, Naumann J, Sattler E. Analysis of martensitic transformation in 304 type stainless analysis of martensitic transformation in 304 type stainless steels tensile tested in high pressure hydrogen atmosphere by means of XRD and magnetic induction. International Journal of Hydrogen Energy 2012;37:3567–72.
[19] Marchi CS, Somerday BP, Tang X, Schiroky GH. Effects of alloy composition and strain hardening on tensile fracture of hydrogen-precharged type 316 stainless steels. International Journal of Hydrogen Energy 2008;33(2):889–904.
[20] Zhang L, Wen M, Imade M. Effect of nickel equivalent on hydrogen gas embrittlement of austenitic stainless steels based on type 316 at low temperatures. Acta Materialia 2008;56(14):3414–21.
[21] Louthan MR, Caskey GR, Donovan JA, Rawl DE. Hydrogen embrittlement of metals. Materials Science and Engineering 1972;10(6):357–68.
[22] Brooks JA, West AJ. Hydrogen induced ductility losses in austenitic stainless-steel welds. Metallurgical Transactions A – Physical Metallurgy and Materials Science 1981;12(2):213–23.
[23] Talonen J, Hanninen H. Formation of shear bands and strain-induced martensite during plastic deformation of metastable austenitic stainless steels. Acta Materialia 2007;55(18):6108–18.
[24] Michler T, Naumann J. Hydrogen environment embrittlement of austenitic stainless steels at low temperatures. International Journal of Hydrogen Energy 2008;33(8):2111–22.
[25] Michler T, Yukhimchuk AA, Naumann J. Hydrogen environment embrittlement testing at low temperatures and high pressures. Corrosion Science 2008;50(12):3519–26.
[26] Perng TP, Altstetter CJ. Hydrogen effects in austenitic stainless-steels. Materials Science and Engineering: A 1990;129(1):99–107.
[27] West AJ, Louthan MR. Hydrogen effects on the tensile properties of 21-6-9 stainless steel. Metallurgical Transaction A 1982;13:2049–58.
[28] Nibur KA, Somerday BP, Balch DK, San Marchi C. The role of localized deformation in hydrogen-assisted crack propagation in 21Cr-6Ni-9Mn stainless steel. Acta Materialia 2009;57(13):3795–809.
[29] Nibur KA, Bahr DF, Somerday BP. Hydrogen effects on dislocation activity in austenitic stainless steel. Acta Materialia 2006;54:2677–84.
[30] Nibur KA, Somerday BP, San Marchi C, Balch DK. Effects of strength and microstructure on hydrogen-assisted crack propagation in 22Cr-13Ni-5Mn stainless steel forgings. Metallurgical and Materials Transactions A 2010;41(13):3348–57.
[31] Michler T, Naumann J. Hydrogen embrittlement of Cr-Mn-N-austenitic stainless steels. International Journal of Hydrogen Energy 2010;35(3):1485–92.
[32] Gavriljuk VG, Tyshchenko AI, Bliznuk VV, Yakovleva IL, Riedner S, Berns H. Cold work hardening of high-strength austenitic steels. Steel Research 2008;79(6):413–22.
[33] Gavriljuk VG, Shanina BD, Berns H. Ab initio development of a high-strength corrosion-resistant austenitic steel. Acta Materialia 2008;56:5071–82.
[34] Berns H, Hussong B, Riedner S, Wischnowski F. Effect of carbon on stainless austenitic FeCrMnN castings. Steel Research 2010;3(81):245–51.
[35] McIntyre DR. Ranking materials for extreme sour gas service using the slow strain rate method. In: Raymond L, editor. Hydrogen embrittlement. ASTM; 1988. p. 178–89.
[36] Birnbaum HK, Sofronis P. Hydrogen-enhanced localized plasticity – a mechanism for hydrogen-related fracture. Materials Science and Engineering: A 1994;176(1–2):191–202.
[37] Lecoester F, Chene J, Noel D. Hydrogen embrittlement of the Ni-base alloy 600 correlated with hydrogen transport by dislocations. Materials Science and Engineering: A 1999;262(1–2):173–83.
[38] Sun D, Han G, Vaodee S, Fukuyama S, Yokogawa K. Tensile behaviour of type 304 austenitic stainless steels in hydrogen atmosphere at low temperatures. Materials Science and Technology 2001;17(3):302–8.
[39] ASTM International. Standard practice for slow strain rate testing to evaluate the susceptibility of metallic materials to environmentally assisted cracking 2006.
[40] Michler T, San Marchi C, Naumann J, Weber S, Martin M. Hydrogen environment embrittlement of stable austenitic steels. International Journal of Hydrogen Energy 2012;37(21):16231–46.
[41] San Marchi C, Nibur K, Balch D, Somreday B, Tang X, Schiroki H, et al. Effects of hydrogen on materials: proceedings of the 2008 international hydrogen conference. ASM International 2009;2009:88–96.
[42] Tabata T, Birnbaum HK. Direct observations of hydrogen enhanced crack propagation in iron. Scripta Metallurgica 1984;18:231.

[43] Robertson IM, Birnbaum HK. An HVEM study of hydrogen effects on the deformation and fracture of nickel. Acta Metallurgica 1986;34:353.
[44] Ulmer DG, Altstetter CJ. Hydrogen-induced strain localization and failure of austenitic stainless steels at high hydrogen concentrations. Acta Metallurgica et Materialia 1991;39(6):1237–48.
[45] Abraham DP, Altstetter CJ. Hydrogen-enhanced localization of plasticity in an austenitic stainless steel. Metallurgical and Materials Transactions A 1995;26(11):2859–71.
[46] San Marchi C, Michler T, Nibur KA, Somerday BP. On the physical differences between tensile testing of type 304 and 316 austenitic stainless steels with internal hydrogen and in external hydrogen. International Journal of Hydrogen Energy 2010;35(18):9736–45.
[47] Saunders N, Miodownik AP. CALPHAD – calculation of phase diagrams: a comprehensive guide. In Pergamon materials series, vol. 1. Oxford: Pergamon; 1998.
[48] Lukas HL, Fries SG, Sundman B. Computational thermodynamics: the Calphad method, vol. 2007: Cambridge University Press.
[49] Spencer PJ. A brief history of Calphad. CALPHAD – Computer Coupling of Phase Diagrams and Thermochemistry 2008;32(1):1–8.
[50] Bain EC, Paxton HW. Alloying elements in steel. Am. Soc. for Metals; 1966.
[51] Nohara K, Ono Y, Ohashi N. Composition and grain size dependencies of strain-induced martensitic transformation in metastable austenitic stainless steels. ISIJ International 1977;63(5):212–22.
[52] Schramm RE, Reed RP. Stacking-fault energies of 7 commercial austenitic stainless-steels. Metallurgical Transactions A – Physical Metallurgy and Materials Science 1975;6(7):1345–51.
[53] Brofman PJ, Ansell GS. Effect of carbon on stacking-fault energy of austenitic stainless-steels. Metallurgical Transactions A – Physical Metallurgy and Materials Science 1978;9(6):879–80.
[54] Vitos L, Nilsson JO, Johansson B. Alloying effects on the stacking fault energy in austenitic stainless steels from first-principles theory. Acta Materialia 2006;54(14):3821–6.
[55] Dumay A, Chateau JP, Allain S, Migot S, Bouaziz O. Influence of addition elements on the stacking-fault energy and mechanical properties of an austenitic Fe-Mn-C steel. Materials Science and Engineering: A 2008;483–484:184–7.
[56] Ronevich JA, Kim SK, Speer JG, Matlock DK. Hydrogen effects on cathodically charged twinning-induced plasticity steel. Scripta Materialia 2012;66:956–9.
[57] Rhodes CG, Thompson AW. The composition dependence of stacking-fault energy in austenitic stainless-steels. Metallurgical Transactions A – Physical Metallurgy and Materials Science 1977;8(12):1901–6.
[58] Martin M, Weber S, Izawa C, Wagner S, Pundt A, Theisen W. Influence of machining-induced martensite on hydrogen-assisted fracture of AISI type 304 austenitic stainless steel. International Journal of Hydrogen Energy 2011;36(17):11195–206. URL, http://www.sciencedirect.com/science/article/pii/S0360319911013826.
[59] Talonen J, Aspegren P, Hanninen H. Comparison of different methods for measuring strain induced alpha-martensite content in austenitic steels. Materials Science and Technology 2004;20(12):1506–12.
[60] Narita N, Altstetter CJ, Birnbaum HK. Hydrogen-related phase transforamtions in austenitc stainless steels. Metallurgical Transaction A 1982;13:1355–65.
[61] Thermo-Calc Software AB. Thermo-calc user's guide versions: Foundation of Computational Thermodynamics.
[62] Sundmann B, Shi P, Bratberg J. Tcfe6: Tcs steels/Fe-alloys database v6 Juni 2008.
[63] Dieter GE, Bacon DJ. Mechanical metallurgy. SI Metric ed. London and New York: McGraw-Hill; 1988.
[64] Reed-Hill RE, Abbaschian R. Physical metallurgy principles. 3rd ed. Boston: PWS-Kent Pub.; 1992.
[65] ASM International (Ed.). Volume 12-fractography; 1992.
[66] Michler T, Lee Y, Gangloff RP, Naumann J. Influence of macro segregation on hydrogen environment embrittlement of SUS 316L stainless steel. International Journal of Hydrogen Energy 2009;34(7):3201–9.
[67] Weber S, Martin M, Theisen W. Impact of heat treatment on the mechanical properties of AISI 304L austenitic stainless steel in high-pressure hydrogen gas. Journal of Materials Science 2012;47(16):6095–107.